Experimental study and discrete element analysis on lateral resistance of windblown sand railway

Zhang, Zhihai; Xiao, Hong; Wang, Yang; Fang, Jia; Nadakatti, M. M.; Wang, Haoyu

Important note
To cite this publication, please use the final published version (if applicable).
Please check the document version above.

Check for updates

Experimental study and discrete element analysis on lateral resistance of windblown sand railway

Zhihai Zhang [a,b], Hong Xiao [a,b,*], Yang Wang [a,b], Jia Fang [a,b], M.M. Nadakatti [c], Haoyu Wang [d]

[a] School of Civil Engineering, Beijing Jiaotong University, Beijing 100044, China
[b] Beijing Key Laboratory of Track Engineering, Beijing Jiaotong University, Beijing 100044, China
[c] Department of Mechanical Engg., KLSGIT, Belgaum, Karnataka 590008, India
[d] Engineering Structures Department, Delft University of Technology, the Netherlands

ABSTRACT

The lateral resistance of ballast bed is an important parameter to prevent track expansion and maintain track stability. The invasion of sand particles can cause the change of lateral resistance of ballast bed and affect the stability of track structure, but little attention has been paid to the change characteristics of nonlinear lateral resistance of sandy ballast bed. In this paper, the field tests on the lateral resistance of windblown sand ballast bed were carried out to establish a multiscale three-dimensional discrete element model of sleeper-ballast bed. A systematic analysis on the evolution of lateral resistance, resistance to lateral deformation, micro-contact characteristics and lateral stability of ballast bed is performed. The results show that sand intrusion can increase the lateral resistance of ballast bed, which is approximately 40 % higher than that of clean ballast bed. In nonlinear strengthening stage and yield stage, the enhancement effect of sand particles on the lateral resistance of ballast bed is relatively weaker in comparison with the linear growth stage. With the increase in sand intrusion depth, the lateral resistance and resistance work of ballast bed both gradually go up, and the contribution of ballast shoulder to lateral resistance tends to play a leading role. Sand intrusion can increase the lateral stiffness of ballast bed and reduce the elasticity of track structure. Therefore, the maintenance operation should be carried out in time for the section with severe sandstorm.

Introduction

The granular ballast bed has many advantages like low construction cost, good elasticity, convenient maintenance and high flexibility [1,2]. It is widely used all over the world, especially in desert environment having complex climatic conditions in places like Baotou-Lanzhou railway and Lanzhou-Xinjiang Railway in China, British military railway, Aus to Lüderitz Railway in Germany, The Hejaz Railway in Saudi Arabia, etc. [3].

The railway ballast bed is a structural body constructed by stacking and compacting crushed stones ballast with varying particle sizes, in which there are a large number of voids. Under the impact vibration of the external environment and train, sand particles can invade the ballast bed continuously to fill the ballast voids, destroy the geometry of the line and change the ballast bed elasticity. This will result in defects like the ballast bed hardening, distorted joint, twist, etc., which can have severe implications on the operational safety [4]. As a result, in-depth study on

the influence of sandstorm environment on the service quality of crushed stone ballast bed is of great significance. It will ensure scientific maintenance and timely repair of railways and also helps in safe and stable operation of trains in desert areas. A typical windblown sand railway line in Northwest China is shown in Fig. 1.

(1) Studies on resistance characteristics of the ballast bed

The crushed stone ballast bed is a non-uniform, particle self-aligning structural body with significant anisotropy. To bear and disperse the longitudinal, transverse and vertical forces transmitted by trains to sleepers, it mainly depends on the contact, occlusion, friction and unique energy dissipation mechanism among particles. It plays a vital role in restraining track frame and also in maintaining the track stability [5]. Adequate lateral resistance of the ballast bed is a key factor to prevent excessive lateral movement of ballast track sleepers and track buckling of continuously welded rail to ensure the lateral stability of the

---

Fig. 1. Windblown sand railway line in Northwest China.

track [6]. With further developments in high-speed and heavy haul railway lines, the requirements for resistance of the ballast bed to lateral loads is found to be continuously increasing [7]. At the same time, crushed stone ballast bed has strong nonlinearity, whose mechanical properties are vastly different from those of common solids and fluids, with extremely complex bearing and shearing properties [8–10]. Many simulation studies have been done by researchers to analyze the characteristics and variations in nonlinear lateral resistance of the ballast bed. Le Pen and Powrie [8] opined that, the contribution from sleeper bottom surface, crib ballast and ballast shoulder to the lateral resistance was 26–35%, 37–50% and 15–37%, respectively. Jing *et al.* [11–13] conducted lateral resistance tests of end-anchorage reinforcement sleeper, ladder-shaped sleeper and polyurethane-mixed ballast bed sleeper. They developed a discrete element model for the ballast bed to analyze the internal relations between different types of sleeper-ballast beds and lateral resistance. The results showed that adoption of new sleeper-ballast bed structure could effectively improve the lateral resistance of ballast beds. Esmaeili *et al.* [14] analyzed the effect of different geogrid layers on the ballast bed reinforcement through laboratory sleeper lateral resistance tests. The studies indicated that the ballast layer reinforced with one and two geogrids increased lateral resistance of single sleeper by 31% and 42% respectively. Guo *et al.* [15] conducted laboratory tests on three kinds of friction sleepers with traditional sleepers in terms of lateral resistance. The studies revealed the variation of lateral resistance through numerical simulation. The results showed that the rough texture of the sleeper bottom surface could effectively enhance the interaction with ballast particles, which could increase the lateral resistance by a maximum of 32%. Kish *et al.* [16,17] obtained the load formula suitable for the calculation of track stability through the ballast bed lateral resistance test. Kabo [18] used elastic–plastic model to simulate and analyze the deformation by considering lateral resistance in 3-D finite element software to get the internal relationship for various displacement values and lateral resistance of the ballast bed. Zeng *et al.* [19] analyzed the influence of ballast gradation, sleeper depth, slope and ballast shoulder width on the variation of lateral resistance of the ballast bed through field tests and discrete element model.

(2) Studies on desert railway ballast bed

Tolou Kian *et al.* [20–22] established a 3-D finite element simulation model based on field experiments and extensive laboratory shear tests with varying sand content. The analysis was also done on the influence of sand content friction angle and deformation modulus of ballast. Zakeri *et al.* [23–25] carried out field experiments in desert areas and proposed a 2-D finite element model for analyzing support stiffness of the ballast bed and load sharing ratios. They opined that the support stiffness of the ballast bed and sharing ratios increased with increase in

sand content. Esmaeili *et al.* [26–28] analyzed the influence of TDA (Tire Derived Aggregate) on the mechanical properties of the ballast bed with sand by field tests. Sadeghi *et al.* [29–30] conducted shear and plate load experiments on ballast samples with varying levels of sand and water content, discussed the influence of wet sand intrusion on the mechanical characteristics of the ballast bed. The authors proposed that that geogrid can significantly improve the shear strength and vertical stiffness of sand ballast bed. Tennakoon *et al.* [32] studied the influence of fine particle content on the permeability of ballast [31]. Ionescu *et al.* [34] analyzed the deformation, deterioration and damping characteristics of the ballast bed with sand [33].

(3) Research gaps in studies conducted so far

From the studies published in the literature, it could be concluded that the research on lateral resistance of the ballast bed mainly focuses on clean ballast bed, involving interfering factors, enhancement measures, structure and load characteristics. It could also be observed that the research on lateral resistance of the ballast bed in desert area is almost insignificant. The existing studies have analyzed the impact of sand intrusion on the mechanical properties of the ballast bed, but they mainly focused on shear strength, support stiffness, reinforcement measures and permeability. Studies did not reveal the impact of the interaction between sand particles and ballast on the lateral resistance characteristics of the ballast bed from mesoscopic point of view.

Based on the research gaps identified, the present study compares and analyzes the variation of lateral resistance between windblown sand ballast bed and clean ballast bed by conducting experiments on lateral resistance. The influence of sand intrusion on the evolution characteristics of the ballast bed resistance is revealed from macro-mesoscopic analysis by utilizing the already established 3-D discrete element model for lateral resistance in ballast bed with sand which could provide theoretical support for the construction, operation and maintenance of desert railway.

Material and method

Ballast and sleeper material properties

To study the influence of sand intrusion on the lateral resistance of the ballast bed, the single sleeper pull-out tests are carried out in the windblown sand section (Ballast voids are almost completely filled with sand) and the clean section. The test line is Class I section of China Railway in which ballast material is basalt gravel. The Los Angeles Abrasion (LAA) rate is 23%, and the standard aggregate impact
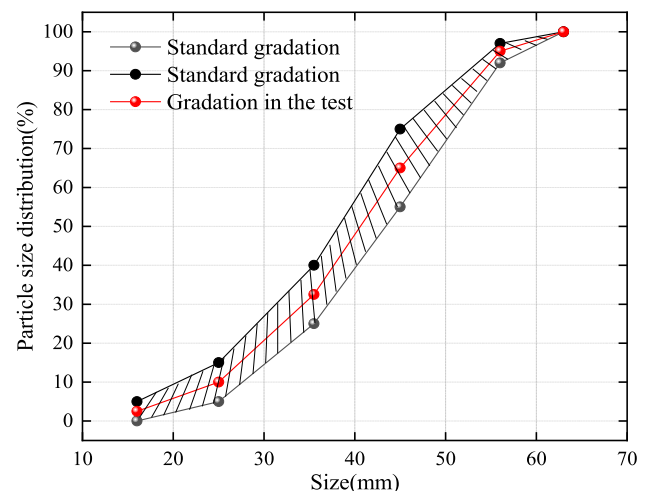

Fig. 2. Gradation of ballast particles (Grade I).

toughness IP (internal pressure) is 97. The ballast particles size gradation is shown as the red curve in Fig. 2. The track structure system is composed of crushed stone ballast bed, new type-II concrete sleepers, bullet type-II fasteners (China's railway fasteners, including two important parameters of buckle pressure and stiffness) and CHN60N (60.64 kg/m) rail, in which the section size parameters of the ballast bed are mentioned in Table 1. The detailed dimensions of new type-II concrete sleepers are mentioned in Table 2.

Test apparatus and procedures

In order to avoid the interference between the mechanical states of adjacent sleepers in the test process, the interval measurement method is adopted to select five sleepers in the sandstorm section and the clean section for experiment. They are numbered in groups from left to right in turn (Group1 ~ Group 5), as shown in Fig. 3. From the Fig. 3, it can be seen that the test system is consisting of hydraulic jack, pressure sensor, reacting equipment, support block, dial indicator, high-precision displacement meter, two supports and a data collection instrument, which mainly measures the lateral resistance of the ballast bed and the lateral displacement of the sleeper. The installation process of the measuring equipment required in the test is shown in Fig. 4.

Before the test, it is necessary to remove the fasteners and pads on the test sleeper. Install the hydraulic jack, pressure sensor, reacting equipment and support block in horizontal direction at one end of the sleeper to apply counterforce to the sleeper, as shown in Fig. 4(d). Then, at the other end of the sleeper, a high-precision displacement meter is fixed on the outer side of the rail through Support 2, which is in close contact with the rail to collect the lateral displacement of the sleeper. Moreover, Fig. 4(e) shows that Support 1 and Support 2 are used to install a dial indicator beside the high-precision displacement meter for checking the loading displacement. During the test, multi-level load is applied to the sleeper by artificially controlling the hydraulic jack. When the sleeper moves slowly under the action of horizontal thrust, the data collection instrument records the readings of the high-precision displacement sensor and dial indicator as well as the lateral resistance measured by the pressure sensor. When the load needs to be increased, the next level of load can only be applied after the sleeper displacement value becomes stable. The sleeper displacement interval is 0.2 mm. The sampling interval is 0.2 mm in test, and near the sleeper displacement of 2 mm is densified. Referring to the present studies [35–39], the average value of lateral resistance corresponding to each displacement under each working condition is plotted. The resistance value at the position where the lateral displacement of sleeper is 2 mm is taken as the evaluation value of lateral resistance of the ballast bed under this working condition.

Results and analysis of the field test

The lateral resistance of the ballast bed is an important index to ensure the stability of continuous welded rail in ballast track [5]. The lateral constraint function of ballast beds on sleepers can be divided into bottom constraint of sleeper, end restraint and crib ballast constraint, as shown in Fig. 5. Lr in the figure indicates the lateral resistance of the ballast bed, R_d is the bottom resistance of sleeper, R_z represents the resistance of ballast shoulder, R_c refers to the resistance of crib ballast.

Analysis of ballast bed lateral resistance

In order to analyze the influence of sand intrusion on the lateral resistance of the ballast bed, the relationship curve between sleeper lateral displacement and ballast bed lateral resistance is drawn up, as shown in Fig. 6.

Fig. 6 indicates that with the gradual increase in sleeper displacement, there is a gradual increase in lateral resistance of ballast as well. The lateral resistance of the ballast bed refers to the resistance value when the sleeper is displaced by 2 mm [11–12]. It can be seen from Fig. 6(a) and Fig. 6 (b) that the lateral resistance of five sleepers on the windblown sand ballast bed is between 10.26 kN and 11.76 kN, while that of the clean ballast bed is between 7.29 kN and 8.60 kN. It shows that resistance of the windblown sand ballast bed is considerably greater than that of the clean ballast bed. Fig. 6(c) demonstrates that the average lateral resistance of the windblown sand ballast bed is 11.18kN, and that of the clean ballast bed is 7.93kN, which is approximately 40 % less than that of the windblown sand ballast bed. This shows that the sand invasion can increase the lateral resistance of the ballast bed. The reason is that after the sand particles invade the ballast bed, the number of contacts between the sleeper and the particles inside the ballast is increased. With the cyclic load of the train, the interlocking effect between the ballast-sand particles and the sleeper is enhanced, the friction between the sand particles and the sleeper is increased. And the contact force chain around the sleeper is gradually encrypted, thereby improving the lateral resistance and deformation resistance of the ballast bed.

In order to further study the influence of sand intrusion on the resistance characteristics of the ballast bed, the mean curve of lateral resistance in Fig. 6(c) is divided into three stages namely: linear growth stage, nonlinear strengthening stage and yield stage. The trend variation of each stage is plotted and analyzed, as shown in Table 3.

Table 3. Ballast bed lateral resistance curve fitting formulae

It can be seen from Fig. 6(c) and Table 3 that the lateral resistance of the ballast bed changes as a linear function during the linear growth stage. The change rate of lateral resistance for the windblown sand ballast bed *b* is 39.82kN/mm and for clean ballast bed it is 8.13kN/mm. It is 4.9 times smaller than that of windblown sand ballast bed. It shows that when the ballast voids are completely filled with sand, the sand can bear part of the load, and the ability of the ballast bed to resist lateral deformation can become stronger. This is closely related to the fact that the intrusion of sand particles increases the number of contact between the sleeper and the particles inside the ballast bed, and changes the force transmission mechanism between the sleeper and the ballast bed. In the nonlinear strengthening stage, the lateral resistance of the ballast bed fails to increase gradually, while the lateral displacement of the sleeper tends to increase. In comparison with clean ballast bed, the windblown sand ballast bed could enter the nonlinear strengthening stage with an increased pace. In the yield stage, the lateral load remains basically unchanged but the sleeper displacement still increases. This is because the original contact state between the sleeper and the internal particles of the ballast bed is closely related to the failure under large lateral load.

From the curve fitting formulae for nonlinear strengthening stage and yield stage, it is obvious that the lateral resistance of windblown sand ballast bed changes as a power function and its goodness of fit is 0.996. The clean ballast bed follows a quadratic function pattern, whose goodness of fit is 0.906. Although there are differences in the curve fitting functions of these two types of ballast beds, their changing trends are similar. The trends indicate that sand particles have increased effect

Table 1
Ballast bed properties.

Track type	Sleeper space (mm)	Ballast height(mm)	Top with(mm)	Shoulder Width(mm)	Shoulder height(50 mm)	Slope gradient	Sand content
Sand	600	350	3500	500	50	1:1.75	Full
Clean	600	350	3500	500	50	1:1.75	0

Table 2
Sleeper specifications.

Sleeper type	Bottom surface (cm²)	End surface (cm²)	Mass (kg)	Length (mm)	Section width (mm)			Section height (mm)		
					End	Rail seat	Mid-section	End	Rail seat	Mid-section
New type-II concrete sleepers	6806.25	463	273	2500	294.5	280	250	200	205	175
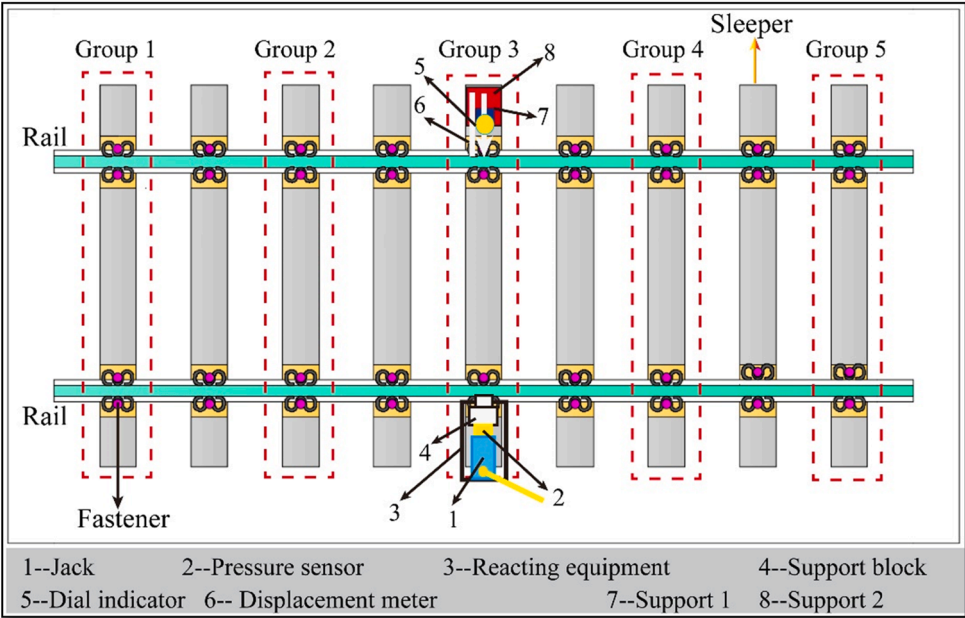
Fig. 3. Schematic diagram of loading and measuring points' selection.
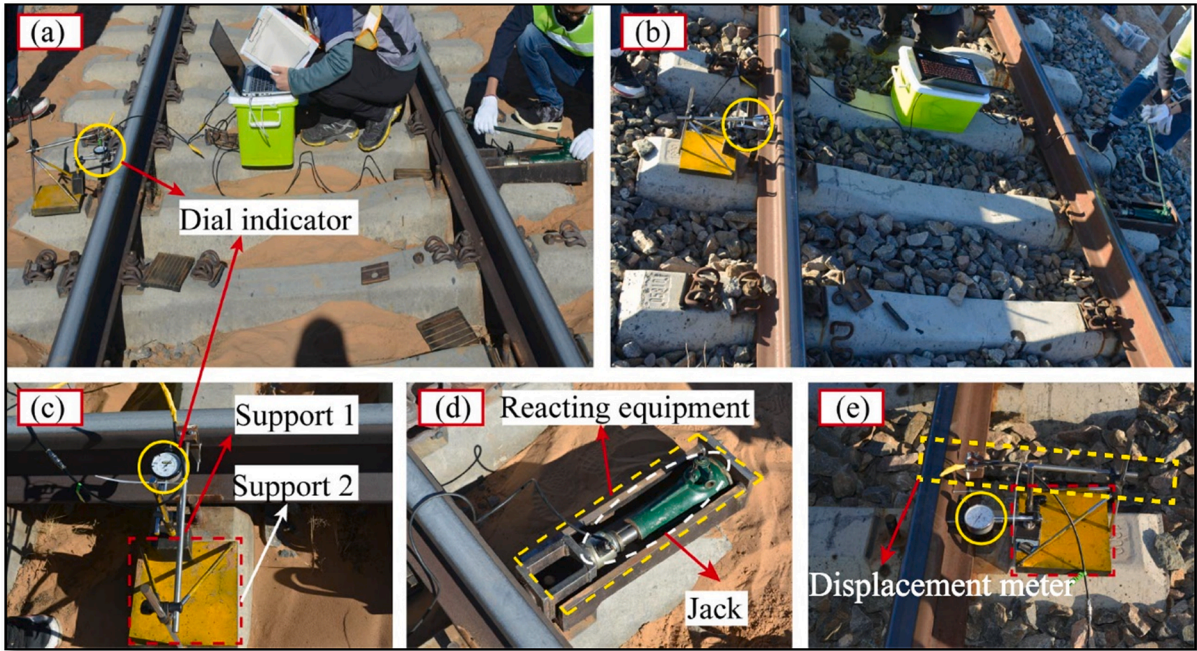
Fig. 4. Installation of test apparatus.

on the lateral resistance of ballast beds in those stages. It may be concluded that in windblown sand ballast bed and clean ballast bed, the variation law of lateral resistance at different stages could be written as polynomial function, as mentioned in Eq. (1).

$$L_r = ax^d + bx + c \qquad (1)$$

Where x is the lateral displacement of sleeper, a, b, c, and d are the resistance change parameters, which could be selected based on
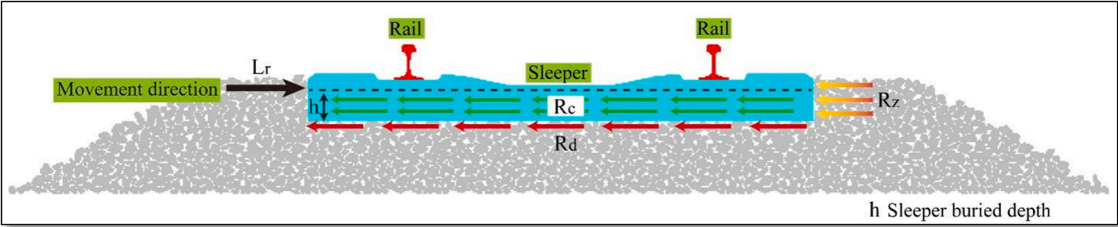
Fig. 5. Composition of ballast bed lateral resistance.
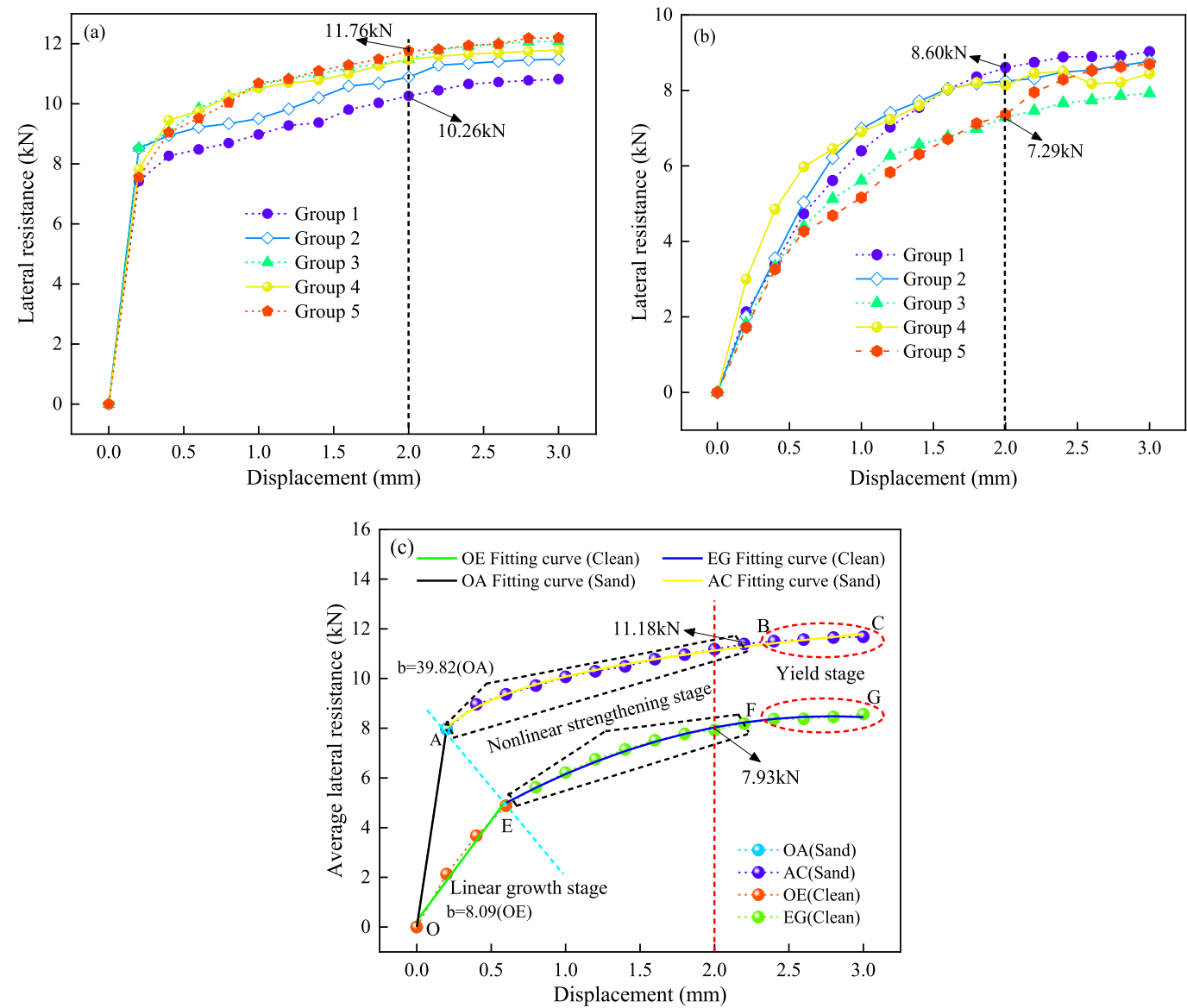
Fig. 6. Results of lateral resistance test: (a) windblown sand ballast bed, (b) clean ballast bed, (c) mean value diagram of lateral resistance.

Table 3
Ballast bed lateral resistance curve fitting formulae.

Type of ballast bed	Plot Equations OA/OE	Parameter	Goodness of fit	AC/EG	Parameter	Goodness of fit
Windblown sand ballast bed	$L_r = c + bx$	$c = 0$ $b = 39.82$	$R^2 = 1.000$	$L_r = ax^d + bx + c$	$a = 10.07$ $b = 0$ $c = 0$ $d = 0.143$	$R^2 = 0.996$
Clean ballast bed		$c = 0$ $b = 8.13$	$R^2 = 0.975$		$a = -0.731$ $b = 4.067$ $c = 2.821$ $d = 2.000$	$R^2 = 0.996$

characteristics of lateral resistance change of the ballast bed.

Analysis on lateral resistance work of ballast bed

In order to further explore the variation of lateral resistance of windblown sand ballast bed, this paper discusses the influence of sand intrusion on the lateral stability of railway lines by utilizing the lateral resistance work of the ballast bed. The lateral resistance work of the ballast bed refers to the area enclosed by the lateral resistance curve of the ballast bed and × axis of cartesian coordinate system [7,36] and could be analyzed using the equation:

$$w_R = \int_0^x L_r(x)dx \qquad (2)$$

Where w_R is the lateral resistance work of the ballast bed, $L_r(x)$ is the lateral resistance-displacement curve and × is the lateral displacement of sleeper.

The resistance work evolution process of windblown sand ballast bed and clean ballast bed are shown in Fig. 7. From Fig. 7(a) and Fig. 7(b). It could be observed that increase of lateral displacement of sleepers will result in gradual increase of the resistance work for both kinds of ballast beds. Among the two kinds of ballast beds, the resistance work of windblown sand ballast bed in linear growth stage is 0.797kN·mm and for non-linear strengthening stage it is 20.295 kN·mm. During yield stage the resistance work of windblown sand ballast bed is 9.231 kN·mm. It is approximately 46 % lower than that of clean ballast bed during linear growth stage. At the same time, it is approximately 83 % and 37 % more than that of clean ballast bed in strengthening stage and yield stage respectively. This shows that the work done by the windblown sand ballast bed to overcome the lateral resistance is mainly concentrated in the nonlinear strengthening stage and yield stage, while the linear growth stage is relatively less.

In Fig. 7(c), when the sleeper displacement is 2 mm, the work done by overcoming the lateral resistance of the windblown sand ballast bed is 18.85 kN·mm and the work by the clean ballast bed is 10.92 kN·mm. The resistance work of the windblown sand ballast bed increases to 73 % in comparison with the clean ballast bed. It could also be observed that greater the displacement of the ballast bed, more work will be needed to overcome the lateral resistance of the ballast bed. Further, it could be inferred that, stronger the anti-interference of the ballast bed results in better the stability. These outcomes are in consistent with the literature [36].
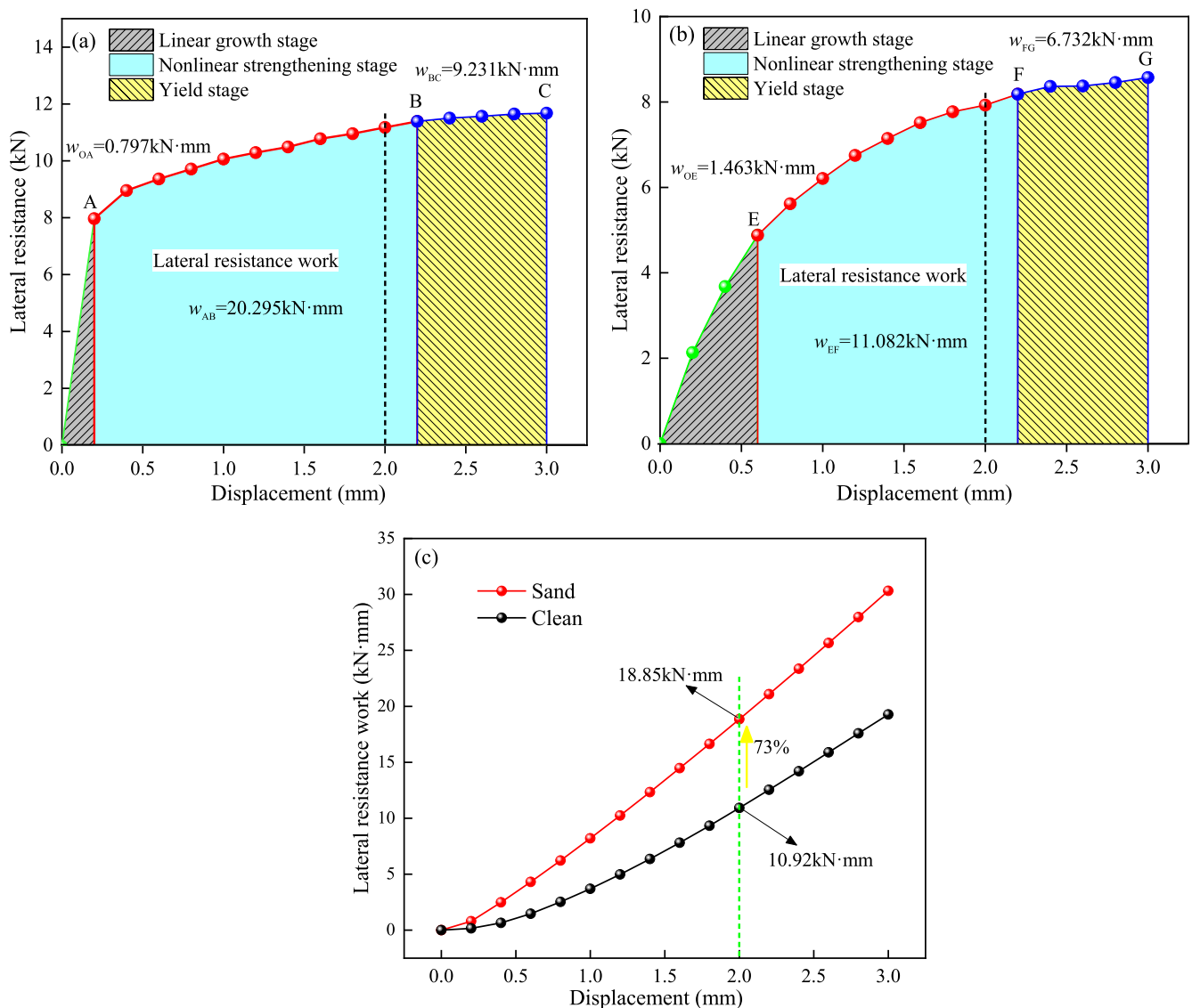

Fig. 7. Evolution process of the ballast bed resistance work: (a) windblown sand ballast bed, (b) clean the roadbed, (c) comparison of the evolution process of resistance work.

Discrete element modeling

Ballast particle model

Ballast particles have varied shapes, sharp edges and remarkable multi-scale effects. For precise development of model and reliable simulation results it is essential that, irregularly shaped ballast particles be restored and reconstructed with utmost accuracy [40–42]. At present, the construction of techniques for 3-D ballast particle model mainly include: laser scanning [43], Fourier analysis method [44] and construction method of ellipsoid surfaces [45]. In order to study the microscopic characteristics of irregular ballast particles, laser scanning method is used in the present analysis to extract 3-D profile of ballast particles, as shown in Fig. 8. In profile extraction, initially ballast particles are placed on the rotating platform of laser scanner for rotary scanning. Then the ballast profile is generated and STL file is derived. This file is imported into the DEM application for the construction of the ballast particle template using particle stacking method [46]. To accurately simulate the characteristics of different ballast particle shapes, 12 typical ballast particle samples are selected for modeling, as shown in Fig. 9.

Sleeper-ballast model

Considering the actual ground condition of the test site, a ballast model with a top surface width of 3500 mm, a thickness of 350 mm and a side slope gradient of 1:1.75 is developed by applying the grade I ballast particle gradation of the red curve in Fig. 2. The discrete element sub-model of new Type-II concrete sleeper with a length of 2500 mm is established by using particle retention method for geometriy and ball element configuration, as shown in Fig. 10 (d). It should be noted that the sand particles' size (0.2 mm ~ 0.8 mm) is much smaller than that of ballast particles (25 mm ~ 63 mm) which has significant cross-scale effect on the model. Hence it is difficult to balance and may cause particle suspension. In order to analyze the discrete element model of windblown sand ballast bed which has balancing difficulty, in the present research, a mixed block of ballast and sand (300 mm × 300 mm × 300 mm) is established in the beginning [4]. Later, the windblown sand ballast bed model is established by block assembly method when the block gets balanced completely [4]. The model contains 21,200 particles in the clump (Ballast) unit and 320,700 particles in the ball (Sand) unit,
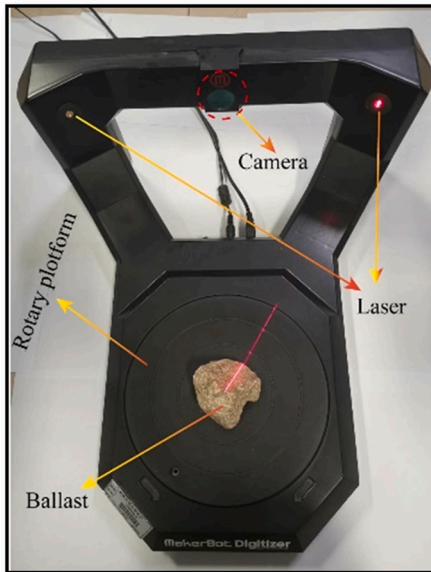

Fig. 8. 3-D Laser scanning.

as shown in Fig. 10 (a). Considering the fact that the particle size has a great influence on the computational efficiency of the model and with reference research conducted so far in this field [4,47], the sand particle size is found to be enlarged by three times. If the minimum particle size of sand is 0.6 mm, the maximum particle size of sand is 3 mm, its average particle size is 1.8 mm. The discrete element model of windblown sand ballast bed and clean ballast bed is shown in Fig. 10. In particular, it should be noted that the density of windblown sand ballast bed is 2200 kg/m^3 in Fig. 10 (a), and the density of clean ballast bed is 1680 kg/m^3 in Fig. 10 (b).

For simulation of the ballast bed lateral resistance, the sleeper speed is set as 0.001 m/s, the computational time interval is set as 1×10^{-8} s and the local damping of particles is set as 0.7 [13]. According to the experimental results mentioned in section 3.1, it could be observed that when the lateral displacement reaches 3 mm, the lateral resistance of the ballast bed is almost stable. Therefore the maximum lateral displacement of sleeper is set as 3 mm. At the same time, the lateral displacement and lateral contact force of sleepers are also monitored.

Contact model and parameters

In the discrete element model, ballast particles are simulated by Clump element. Since the sand particle is small in size, from the current research in related fields [47], ball element is adopted for simulation. The contact between all particles in the ballast model adopts a linear contact model, as shown in Fig. 11.

It can be seen from Fig. 11 that the contact force F between the ballast bed particles mainly includes normal contact force F_n and tangential contact force F_s [48], as mentioned in Eq.3. The normal contact force F_n can be calculated by Eq. (4). The tangential contact force F_s can be calculated by Eq.5.

$$F = F_n + F_s \tag{3}$$

$$F_n = F_n^l + F_n^d \tag{4}$$

$$F_s = F_s^l + F_s^d \tag{5}$$

In these equations, F_s is the normal linear contact force, which can be calculated by Eq. (6), F_n^d is the normal damping force, calculated by Eq. (7), F_s^l is tangential linear contact force, calculated by Eq. (8) and F_s^d is tangential damping force, that could be calculated by Eq. (9).

$$F_n^l = k_n x_n \tag{6}$$

$$F_n^d = (2\beta_n \sqrt{m_c k_n})\dot{\delta}_n \tag{7}$$

$$F_s^l = (F_s^l)_0 - k_s \triangle x_s \tag{8}$$

$$F_s^d = (2\beta_s \sqrt{m_c k_s})\dot{\delta}_s \tag{9}$$

In the above equations, k_n is the normal contact stiffness, k_s is the tangential contact stiffness, x_n is the normal relative displacement, $(F_s^l)_0$ is the tangential contact force in the initial state, $\triangle x_s$ is the tangential displacement increment, β_n and β_s are the critical damping ratios of normal and tangential respectively, m_c is the effective inertial mass, $\dot{\delta}_n$ and $\dot{\delta}_s$ are the normal and tangential of relative velocities [49].

The discriminant conditions for slip between the ballast particles are as follows:

$$F_{smax} = -\mu|F_n| \tag{10}$$

$$|F_s| > F_{smax} \tag{11}$$

In these equations, μ is friction coefficient and F_{smax} is the maximum friction force. When the tangential contact force of sand $|F_s|$ is greater than the maximum friction force, relative slip will occur between particles.
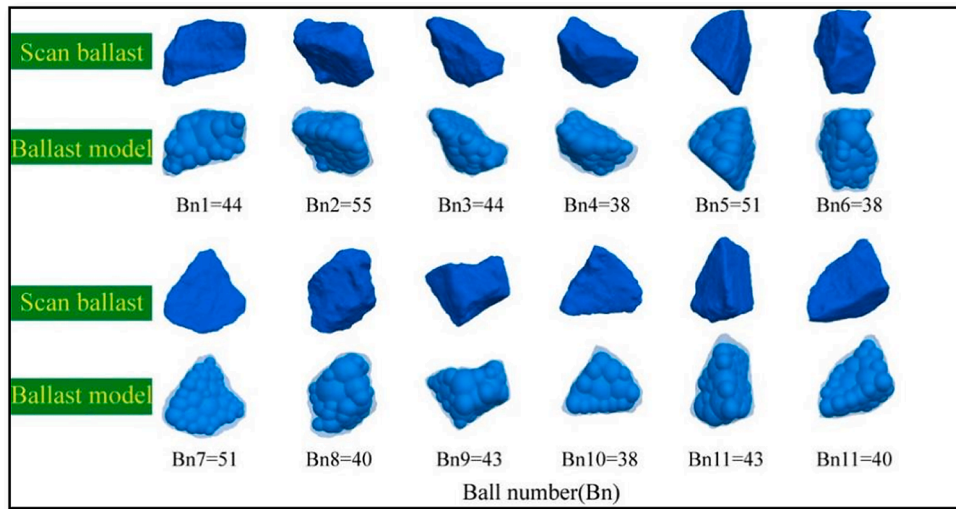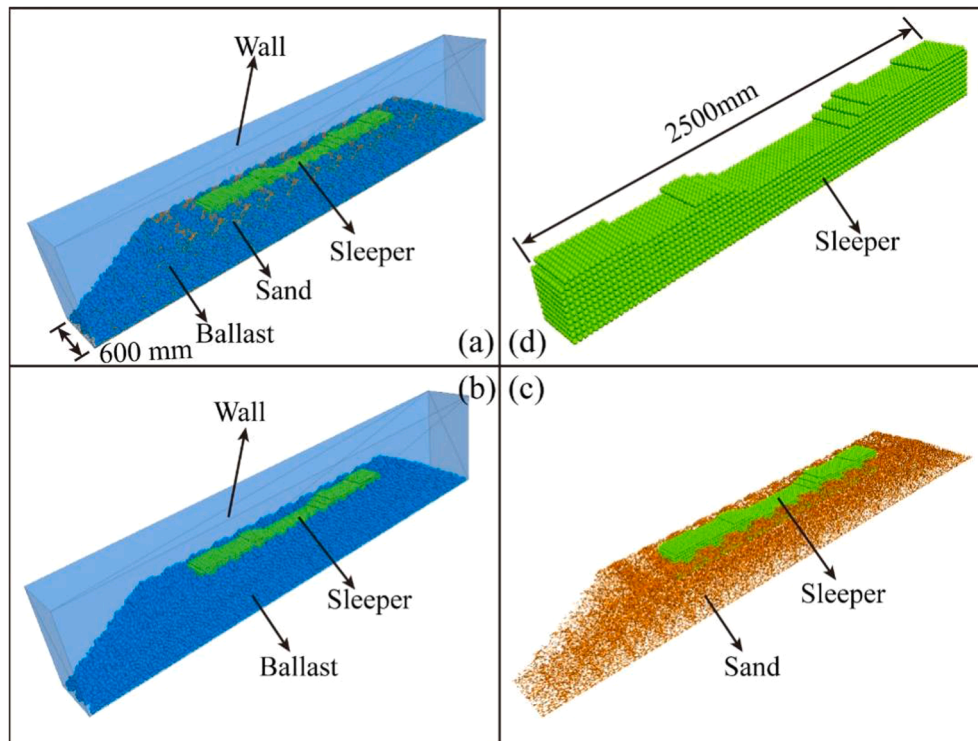
Fig. 9. Ballast particle template.

Fig. 10. Sleeper-ballast discrete element model: (a) windblown sand ballast model, (b) clean ballast bed model, (c) sand-sleeper model; (d) sleeper model.

According to the current studies [4,11,50–51,57–60], along with the field test results of the ballast bed lateral resistance, the contact parameters of the discrete element model are computed, as mentioned in Table 4. The normal and tangential contact stiffness (k_n, k_s) as well as friction coefficient μ between ballast and sand can also be obtained indirectly through the principle of attribute inheritance [49], which could be computed using the equation mentioned below:

$$\frac{1}{k_n} = \frac{1}{k_n^1} + \frac{1}{k_n^2} \qquad (12)$$

$$\frac{1}{k_s} = \frac{1}{k_s^1} + \frac{1}{k_s^2} \qquad (13)$$

$$\mu = min(\mu_1, \mu_2) \qquad (14)$$

In these equations, k_n^1 is the normal contact stiffness of ballast particles, k_n^2 is the normal contact stiffness of sand particles, k_s^1 is the tangential contact stiffness of ballast, k_s^2 is the tangential contact stiffness of sand particles, μ_1 is the friction coefficient of ballast surface and μ_2 is the friction coefficient of sand surface.

Modelling verification

The field measurement results of lateral resistance and resistance work in Section 3 are compared with the simulation results to verify the correctness of the discrete element model, as shown in Fig. 12.
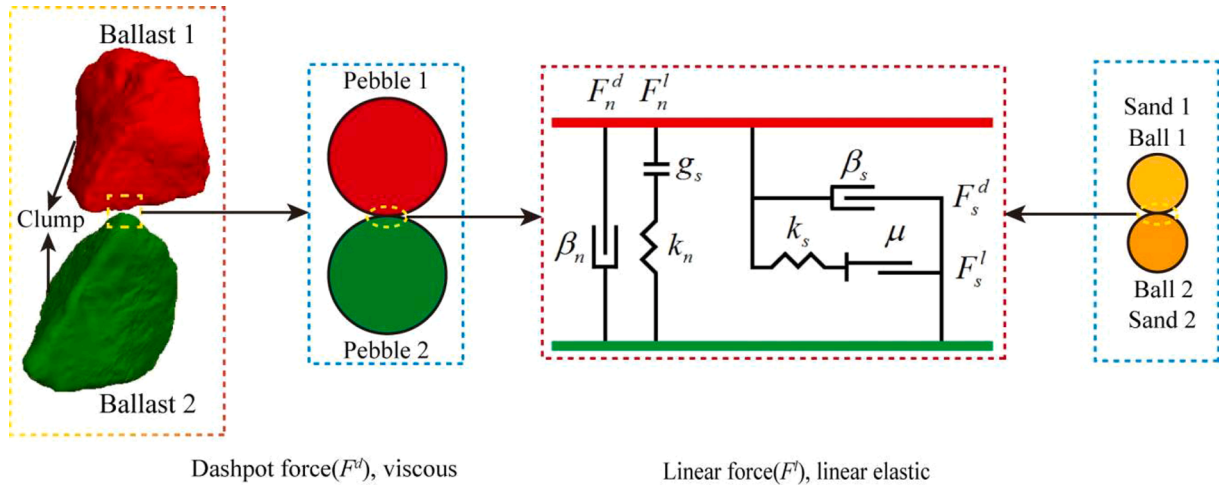
Fig. 11. Contact model.

Table 4
Discrete Element Model Parameters.

Parameter Name	Value
Ballast density (kg/m^3)	2600
Sand density (kg/m^3)	2650
Normal/tangential contact stiffness of ballast (N/m)	$2.5 \times 10^8 / 2 \times 10^8$
Ballast friction coefficient	0.7
Normal/tangential contact stiffness of sand particles (N/m)	$2.0 \times 10^5 / 1.5 \times 10^5$
Friction coefficient of sand particles	0.75
Normal/tangential contact stiffness of wall (N/m)	1.5×10^8

It can be seen from Fig. 12 that when the sleeper displacement increases, the test results and simulation results of lateral resistance and resistance work of two kinds of ballast beds are almost similar. Experimental and simulation results for the lateral resistance of windblown sand ballast bed are 11.18 kN and 11.07 kN respectively. The difference in two values is just 0.98%. For clean ballast bed, the experimental and simulation results are 7.93 kN and 7.61 kN respectively, with difference between the two being 4.04%. It can also be observed from the graphs that, for resistance work of windblown sand ballast bed, the the test result is 18.85 kN·mm and the simulation result is 19.48 kN·mm. The difference between them is almost negligible. For resistance work of

clean ballast bed, the on-sight test result is 10.92 kN·mm while simulation result is 11.92 kN·mm. These are almost close to one-another. In addition, the lateral resistance test values of the two types of ballast beds under the same sleeper displacement are slightly different from the simulation values. Because it is difficult to ensure strict equal interval loading and load stability during the field test, and there are small fluctuations in the loading curve, but it has little impact on the test results. Consequently, in the aspect of the test results and simulation results, the lateral resistance and resistance work of two kinds of ballast beds are similar in numerical change trend and magnitude, showing that it is correct to apply the discrete element model to analyze the lateral resistance characteristics of the ballast bed.

Simulation Analysis

Mesoscopic contact characteristics

The of micro-contact force distribution of chain is an important index which reflects macro mechanics of granular materials [52–53]. For analyzing the influence of sand intrusion on micro-mechanical characteristics of lateral resistance of the ballast bed, the particle information for the main distribution area of contact force is extracted by fish
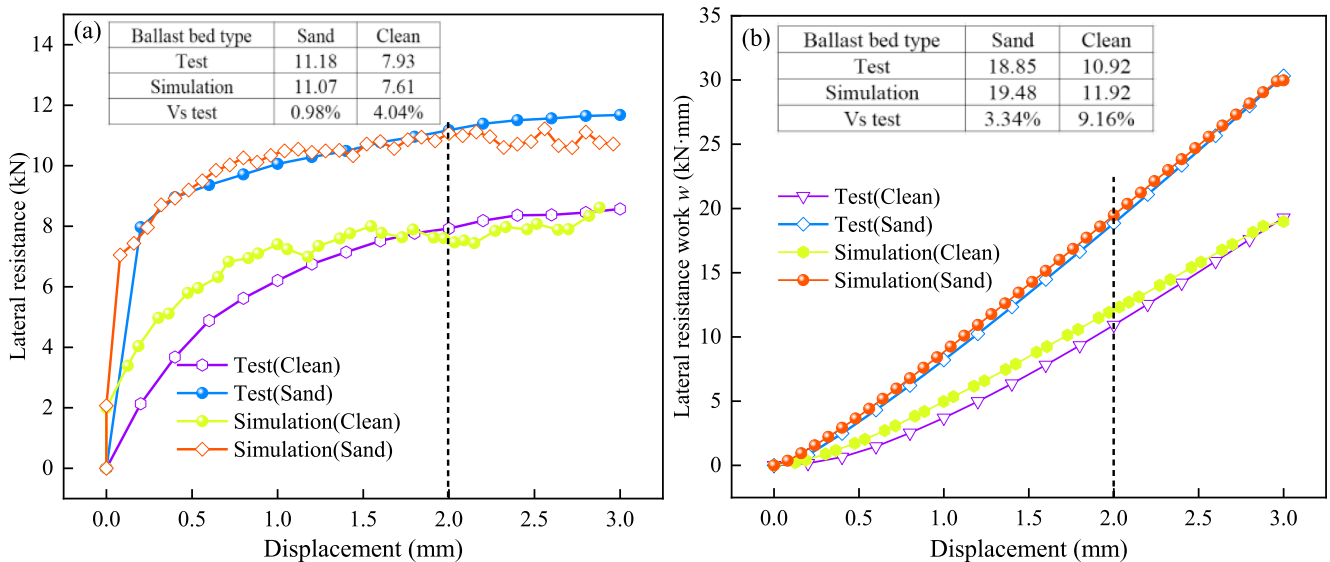

Fig. 12. Test results and simulation results: (a) lateral resistance, (b) lateral resistance work.

language and plots of the micro-contact force chain distribution of ballast beds for two types under varying sleeper lateral displacement values is developed. These are shown in Fig. 13.

Fig. 13 shows that with the increase in sleeper displacement, the contact force between ballast shoulder, crib ballast and sleeper bottom for both types of ballast beds gradually become dense and the skeleton force between them is gradually formed. Specifically, the contact force chain change and force transmission path of ballast shoulder could be clearly distinguished. In addition to the ballast shoulder, the contact force chains in other positions of the windblown sand ballast bed are evenly distributed, while that of the clean ballast bed is distributed in the form of tree roots. It is also seen from the figure that the skeleton force chains play an important role. The reason for relatively uniform force chain distribution of the windblown sand ballast bed is the presence of lot many sand particles in the windblown sand ballast bed which could also share part of the lateral load during the lateral movement of the sleeper.

Through further comparison, it is found that with the increase of sleeper displacement, the maximum contact force of the two kinds of ballast beds increases first and then decreases, which is related to the load stage of the lateral resistance of the ballast bed. In other words, when the lateral resistance of the ballast bed changes from linear growth stage to nonlinear strengthening stage and then to yield stage, the mechanical state in particles gradually change. In the initial stages of loading, few particles participate in the formation of skeleton force chain thereby increasing the contact force between ballast. However, with the increase sleeper displacement, more particles participate in the formation of skeleton force chain and number of contacts gradually increases, resulting in the redistribution of single ballast contact force and reduction of maximum contact force. It could be observed from the results that, the maximum contact force of ballast in windblown sand ballast bed is greater than that in the clean ballast bed under different sleeper displacement values. The maximum difference is approximately 39 % (for 2 mm sleeper displacement). This is primarily because of the fact that, the lateral resistance work of the windblown sand ballast bed is high under the similar displacement levels, requiring additional many energy input from the outside. The input energy changes the contact state of particles and the magnitude of the contact force, so that ballast particles' contact force increases.

The average coordination number and average contact force of particles can be used to find the contact state between particles in the ballast bed. Fig. 14 provides the the average coordination number and average contact force between particles in windblown sand ballast bed and clean ballast bed, in order to further study the influence of the interaction between sand particles and ballast on the micro-

characteristics of the ballast bed resistance.

It can be seen from Fig. 14(a) that the average coordination number of ballast particles in the windblown sand ballast bed is more than that of clean ballast bed. Both ballast beds gradually reach stable stage with the increase in sleeper displacement. This shows that the average contact points' number for the particles in the ballast bed do not change significantly during the increasing value of sleeper displacement. In Fig. 14(b), the average contact force of ballast particles in the windblown sand ballast bed is remarkably higher than that in the clean ballast bed under varying sleeper displacements, while the average contact force of all particles (sand and ballast) in the windblown sand ballast bed is lesser than that in the clean ballast bed. There are more particles participating in resisting the lateral load in the windblown sand ballast bed and hence more load is needed resulting in increase of the average contact force of ballast particles. Also, the windblown sand ballast bed contains a lot of fine sand, whose contact number is much higher than that of the clean ballast bed. As a result, the average contact force of all particles in the windblown sand ballast bed is much less in comparison with clean ballast bed.

Evolution regulation of lateral resistance at different positions

The lateral resistance of the ballast bed is provided by the friction between ballast particles and sleepers, whose resistance is closely related to the friction brought about by ballast shoulders, crib ballast and sleeper bottom. In order to study the influence of sand intrusion on the evolution process of lateral resistance, the lateral resistance values at various sleeper displacement positions are plotted, as shown in Fig. 15.

It can be concluded from Fig. 15 that the sleeper bottom resistance of clean ballast bed is greater than the crib ballast and ballast shoulder under different sleeper displacements, showing that the sleeper bottom resistance is dominant. The ballast shoulder resistance of windblown sand ballast bed is more than the sleeper bottom and crib ballast, which are the main components of total resistance. When the sleeper displacement reaches 2 mm, the ballast shoulder resistance, crib ballast resistance and sleeper bottom resistance of windblown sand ballast bed are 4.44kN, 2.98kN and 3.70kN respectively, which are approximately 121%, 56% and 1% higher than those of the clean ballast bed. This happens because there are a large number of sand particles in the windblown sand ballast bed, especially in the ballast shoulder and crib ballast areas, resulting in increased sand particle contribution towards resistance to the lateral movement of sleepers. By comparing the resistance growth rate at different sections of the windblown sand ballast bed, it is observed that, the ballast shoulder resistance increases the most, which could be attributed to the sand concentration at the ballast
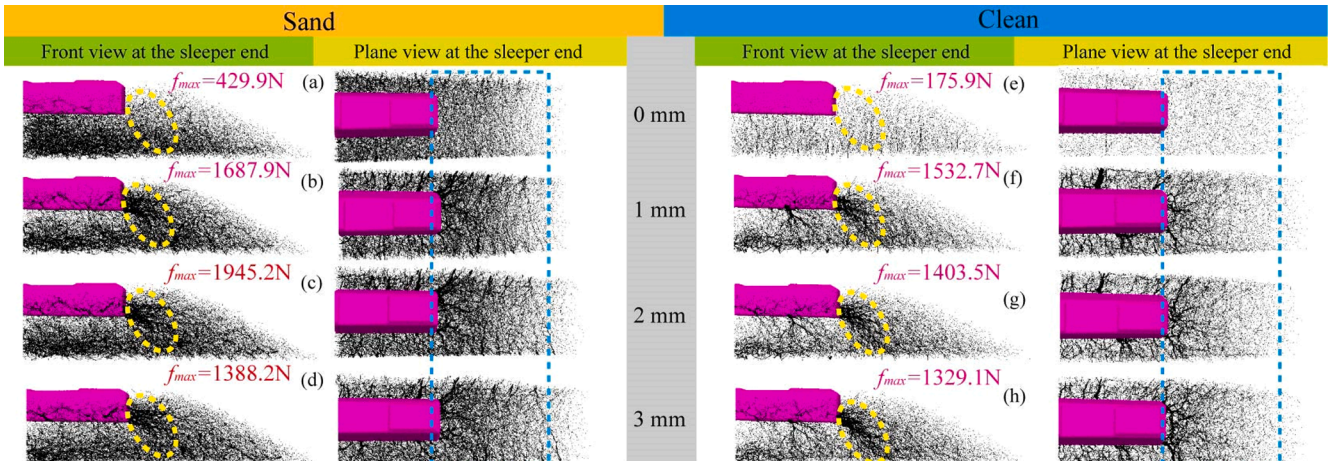

Fig. 13. Micro-contact force chain distribution for various sleeper displacement values: Windblown sand ballast bed: (a) 0 mm, (b) 1 mm, (c) 2 mm, (d) 3 mm. Clean ballast bed : (a) 0 mm, (b) 1 mm, (c) 2 mm, (d) 3 mm.
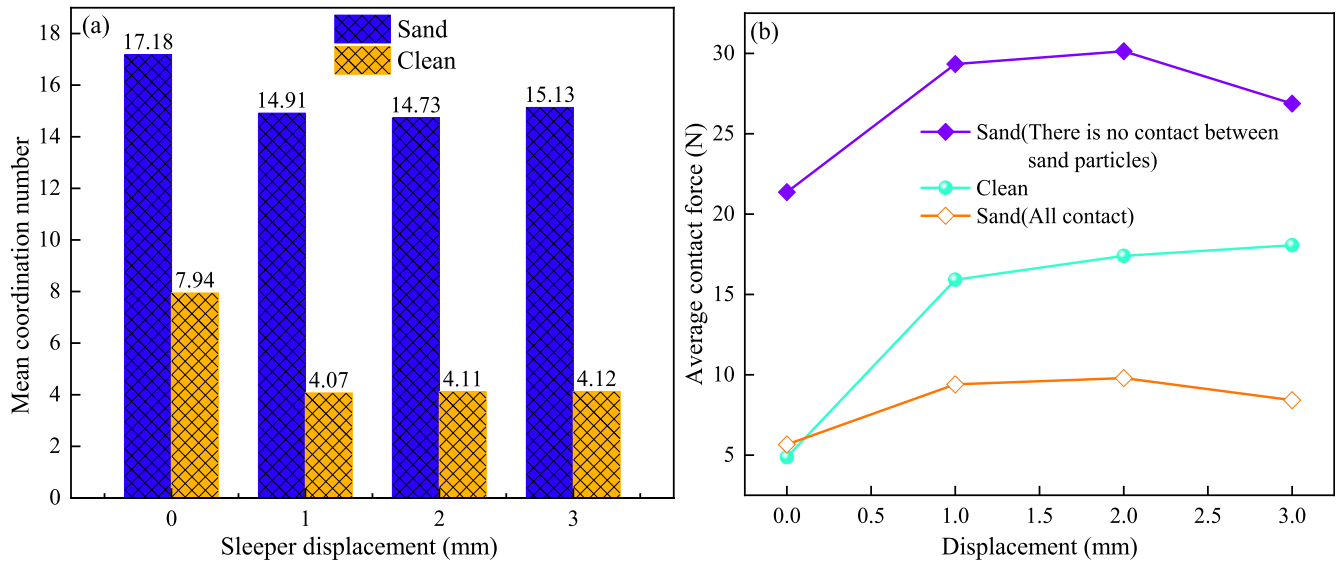
Fig. 14. Average coordination number and contact force of particles in the ballast bed under different sleeper displacements: (a) average coordination number of ballast particles, (b) average contact force.
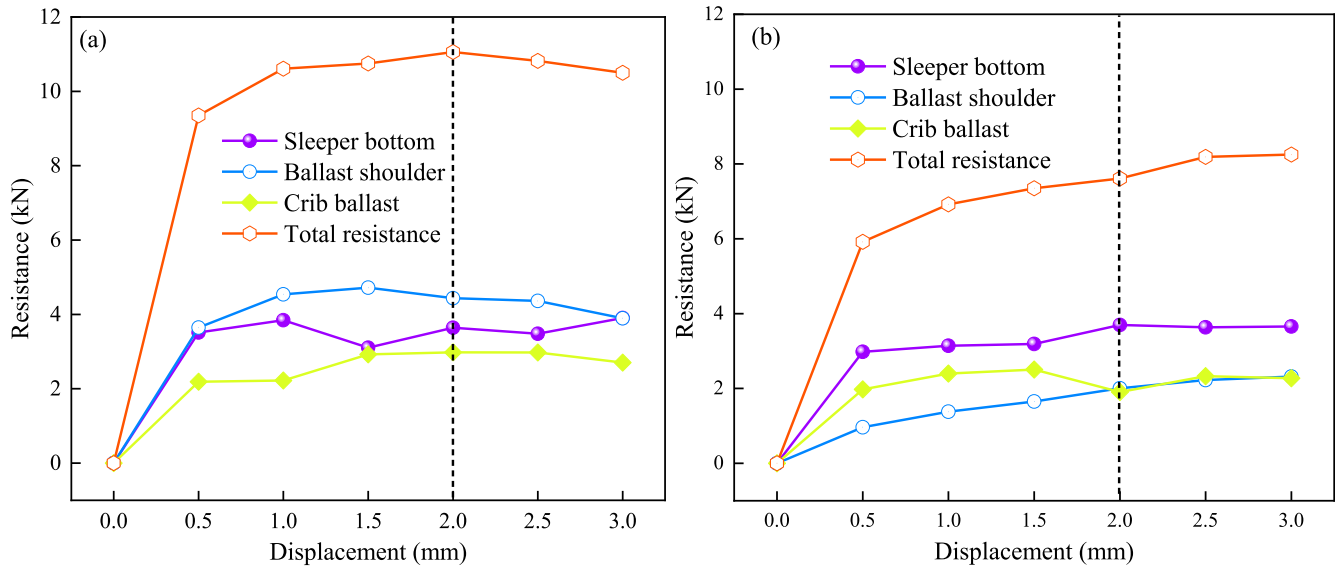

Fig. 15. Change in lateral resistance at various sleeper displacement values: (a) Windblown sand ballast bed, (b) Clean ballast bed.

shoulder.

In order to further study the influence of sand intrusion on different sections of the ballast bed lateral resistance ratio, the resistance sharing ratio of each section under respective displacement value is calculated, as shown in Fig. 16.

It can be observed from Fig. 16 that, for the windblown sand ballast bed, the lateral resistance sharing ratio of ballast shoulder is greater than that of sleeper bottom and crib ballast under different sleeper displacements, while for the clean ballast bed, the resistance sharing ratio of sleeper bottom is greater than that of ballast shoulder and crib ballast. At the 2 mm sleeper displacement, the sleeper bottom resistance sharing ratio of windblown sand ballast bed is approximately 16 % lower than that of clean ballast bed. At the same time the ballast shoulder resistance of windblown sand ballast bed is approximately 14 % higher than that of clean ballast bed. In addition, the crib ballast resistance of windblown sand ballast bed is approximately 2.0 % higher that of clean ballast bed. The data indicate that sand intrusion mainly changes the resistance sharing ratio of sleeper bottom and ballast shoulder but has no influence

on the resistance sharing ratio of crib ballast. This is because the large exposed area of ballast shoulder makes it easy for sand particles to deposit on ballast shoulder to share part of the load. Consequently, the lateral load bearing capacity of ballast shoulder in windblown sand ballast bed will get enhanced.

Analysis on lateral resistance of the ballast bed under varying sand intrusion depths

The sand deposition in the ballast bed is a long process due to the effects of external environment and train load. In order to study the internal relationship between sand intrusion at various depths and lateral resistance of the ballast bed, the influence of sleeper burial depth and ballast shoulder stacking height is taken into consideration. Taking the bottom of the ballast bed as the benchmark (The thickness of the ballast under the sleeper is 0.35 m), the lateral resistance of the ballast bed with the heights of 0.3 m, 0.35 m, 0.4 m, 0.45 m, 0.5 m, and 0.55 m from the sand coverage surface to the bottom of the ballast bed was
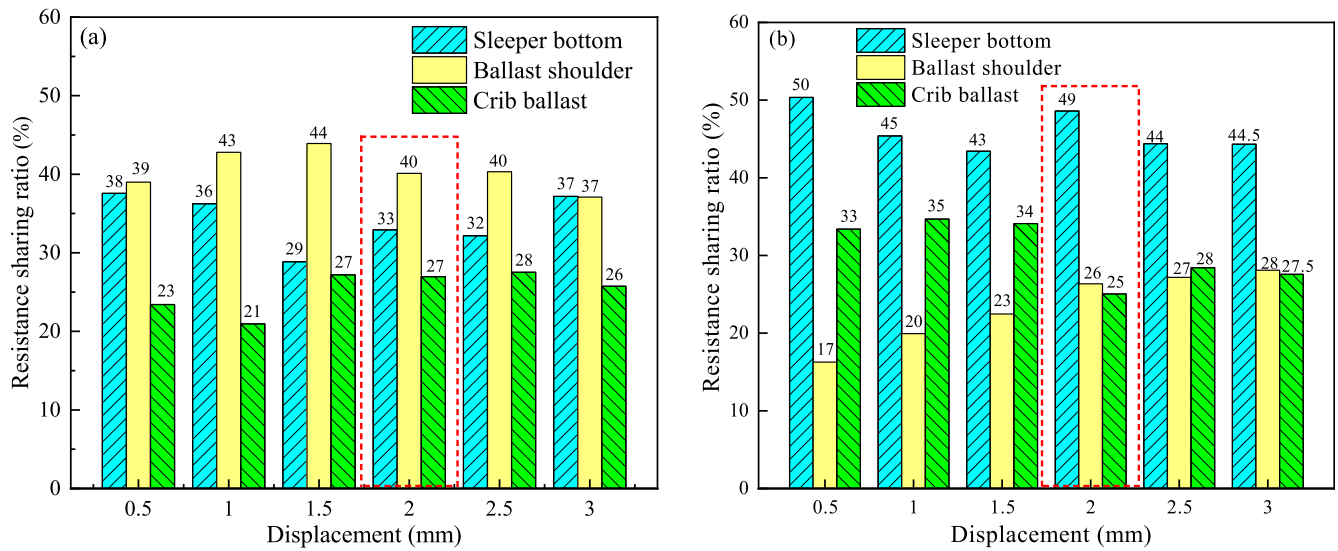
Fig. 16. Change regulation of lateral resistance sharing ratio at different parts: (a) windblown sand ballast bed, (b) clean ballast bed.

calculated, the lateral resistance work is obtained by integration, as shown in Fig. 17.

It can be seen from Fig. 17(a) that the lateral resistance value of the ballast bed under different sleeper displacements increases rapidly at first and then changes slowly with the rise in sand intrusion depth. The deeper the sand intrusion is, greater is the resistance change rate in the linear growth stage and the initial resistance value in the nonlinear strengthening stage. Fig. 17(b) demonstrates that the lateral resistance work of the ballast bed increases almost linearly with the increase in sleeper displacement values under varying sand intrusion depths. Increased sand intrusion depth has an impact on change rate of the ballast bed resistance work, which tends to increase. In order to further study the internal relationship between the sand intrusion depth and the lateral resistance as well as the resistance work of the ballast bed, the resistance and resistance work values of the ballast bed under varying depths of sand intrusion are computed, as shown in Table 5.

It can be seen from Table 5 that, when sand intrusion depth reaches 0.35 m, 0.40 m, 0.45 m, 0.50 m and 0.55 m, lateral resistance can approximately increase by 1 %, 15%, 30%, 35% and 46%. Also, the lateral resistance work approximately increased by 6 %, 26%, 49%, 61%

and 74% respectively, in comparison with the resistance characteristics of the ballast bed at sand intrusion depth of 0.3 m. Therefore, sand intrusion depth plays a more vital role in lateral resistance work than that in lateral resistance, and the more work needs to be done to overcome the resistance of the ballast bed with the increase in sand intrusion depth. So there are more difficulties in changing the mechanical state of the ballast bed. The reason is that with the increase of sand intrusion depth in the ballast bed, the sand content in ballast shoulder and crib ballast gradually goes up and so does the number of particles participating in the actual lateral effect, which leads to the enhanced lateral resistance and resistance work of the ballast bed.

In order to further analyze the influence of sand intrusion depth on the ballast bed lateral resistance characteristics, the lateral resistance values and resistance sharing ratios at different levels of each sand intrusion depths will be calculated at sleeper displacement of 2 mm, as shown in Fig. 18.

It can be seen from Fig. 18 (a) that when the sand intrusion depth is greater than 0.35 m, with the increase of sand intrusion depth, the resistance of ballast shoulder and crib ballast gradually increases, while the resistance of sleeper bottom almost has no obvious change. When the
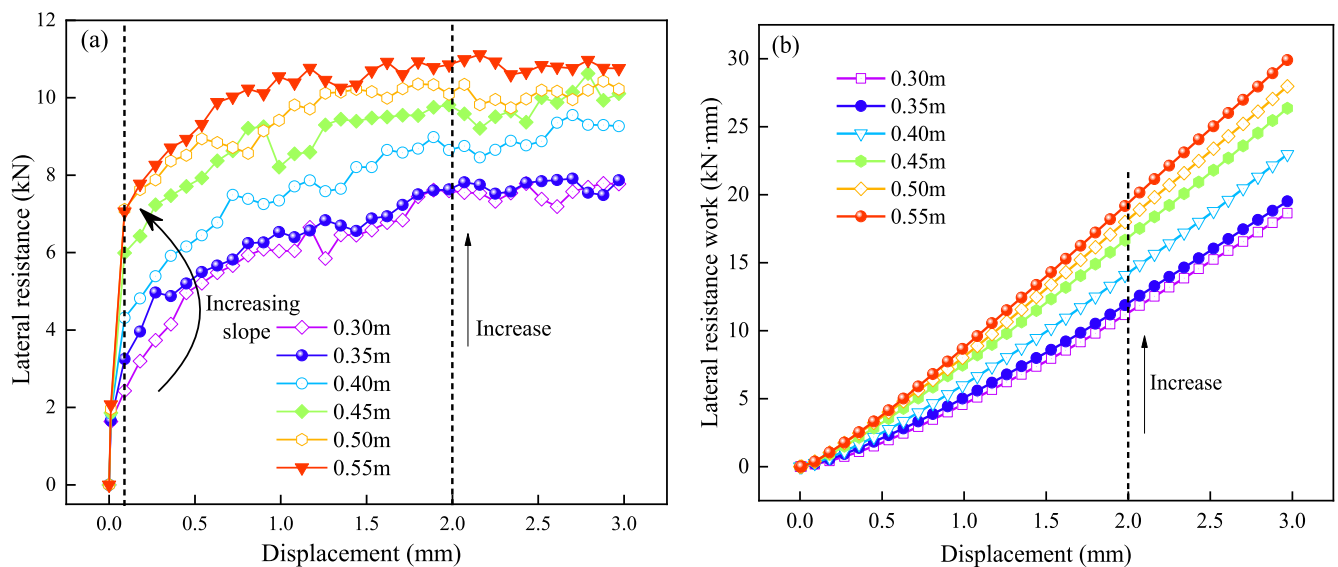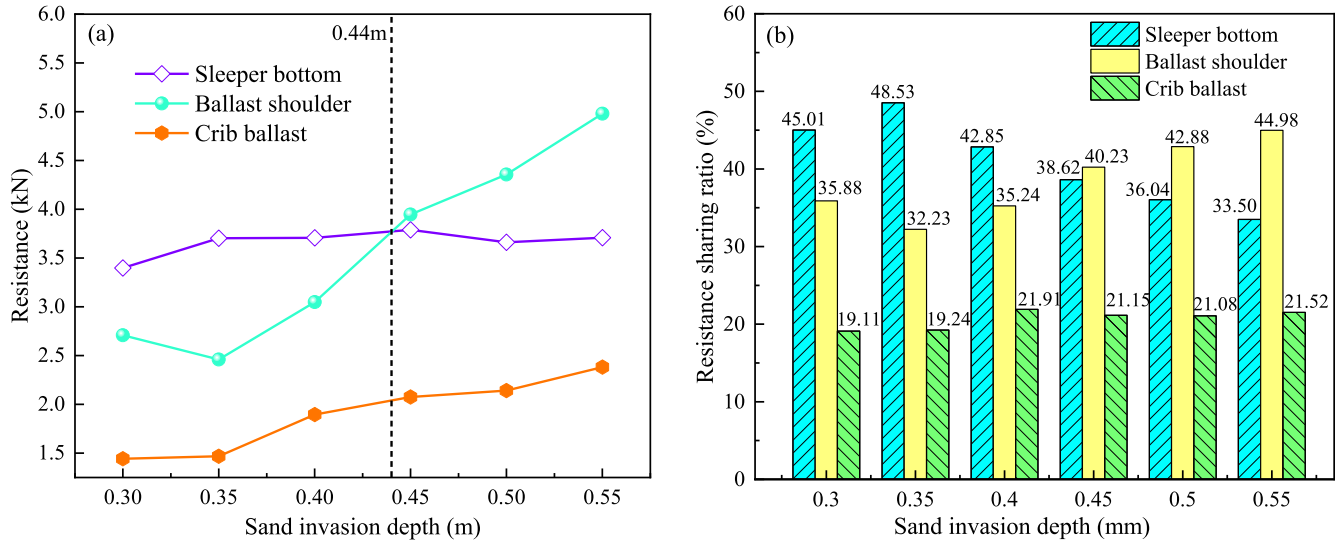

Fig. 17. Changes of lateral resistance and resistance work of the ballast bed under varying depths of sand intrusion: (a) lateral resistance, (b) lateral resistance work.

Table 5
Ballast bed lateral resistance and resistance work under varying depths of sand intrusion.

Projects		Distance from bottom of the ballast bed (m)					
		0.3	0.35	0.40	0.45	0.50	0.55
lateral resistance	Simulated result (kN)	7.55	7.63	8.65	9.81	10.16	11.01
	Growth rate (Vs 0.3 m)	—	1%	15%	30%	35%	46%
lateral resistance work	Simulated result (kN·mm)	11.17	11.87	14.08	16.65	17.99	19.48
	Growth rate (Vs 0.3 m)	—	6%	26%	49%	61%	74%

Fig. 18. Change regulation of lateral resistance sharing ratio and resistance of the ballast bed under varying sand intrusion depths: (a) resistance, (b) resistance sharing ratio.

sand intrusion depth is 0.4 m, the difference between ballast shoulder resistance and crib ballast resistance increases significantly. When the sand intrusion depth is 0.44 m, the ballast shoulder resistance exceeds the sleeper bottom resistance and becomes the main component of the total resistance. It can be seen from Fig. 18(b) that when the sand intrusion depth is greater than 0.35 m, the resistance sharing ratio of sleeper bottom decreases gradually, while the resistance sharing ratio of ballast shoulder increases. This shows that the contribution of sleeper bottom resistance to the total resistance of the ballast bed gradually decreases with the increase in sand intrusion depth. It can be observed that the contribution of ballast shoulder gradually increases, which is the main factor affecting the lateral resistance of the ballast bed. Sand intrusion mainly enhances the ability of ballast shoulder to resist lateral disturbance, but has little effect on sleeper bottom. When the depth of sand invasion exceeds 0.35 m, the sand content of the sleeper bottom is almost unchanged but the sand content of the ballast shoulder and crib ballast increases gradually and also the ability to share the lateral load. However, due to the large exposed area of the ballast bed slope, the sand accumulation at the ballast shoulder is higher than that at the crib ballast. So the resistance sharing ratio of ballast shoulder gradually increases. In addition, with the increase of the sand intrusion depth, the density of the ballast bed slope also increases. With enhanced integrity and stronger lateral restraint ability, the improved the ability of the ballast shoulder to resist lateral disturbance is very well established.

Influence of cyclic load on the ballast bed lateral resistance

Considering the periodicity of temperature and train load, ballast particles participating in sharing lateral load in the ballast bed are in the cyclic change process of "squeezing-relaxing" and the resistance characteristics of the ballast bed are also changing constantly. In order to study the influence of cyclic load amplitude on the ballast bed to resist lateral deformation, references [54–56] are used for applying the lateral cyclic loads with load amplitudes of 5kN, 10 kN, 15 kN and 20kN on sleepers. The lateral force and displacement curves of the ballast bed sleepers for both types with load amplitude of 10kN are also derived, as shown in Fig. 19. The cyclic lateral load equation is as follows:

$$F_c(t) = A(1 + sin(2\pi ft - \frac{\pi}{2}))$$ (15)

In the equation, $F_c(t)$ is the load value changing with time, A is the half amplitude of load and f is the load frequency. Due to the low speed in the sandstorm area, the computed load frequency is 6.8 Hz for fixed wheelbase of 1830 mm on C70E freight and the field running speed of 45 km/h.

In Fig. 19, when the amplitude of cyclic load is 10kN, with the increase of cyclic load time, the lateral displacement value of sleepers on two types of the ballast bed increases gradually. In the repeat load–displacement curve of windblown sand ballast bed, there is an intersection point of the unloading curve of the previous period and the reloading curve of the next period, which is called "common point". Sinha *et. al.* (1964) pointed out that the common point was critical point of elastic and plastic deformations and the slope of loading curve would gradually decrease after passing through the common point, leading to apparent plastic deformation. In order to evaluate the influence of sand intrusion on the ballast bed to resist lateral deformation, the number of common points on two types of ballast beds during 10 cyclic loadings under varying load amplitudes is plotted as shown in Fig. 20.

In Fig. 20, the common point number of the windblown sand ballast bed is almost constant under varying load amplitudes while the common point number of the clean ballast bed gradually decreases and tends to
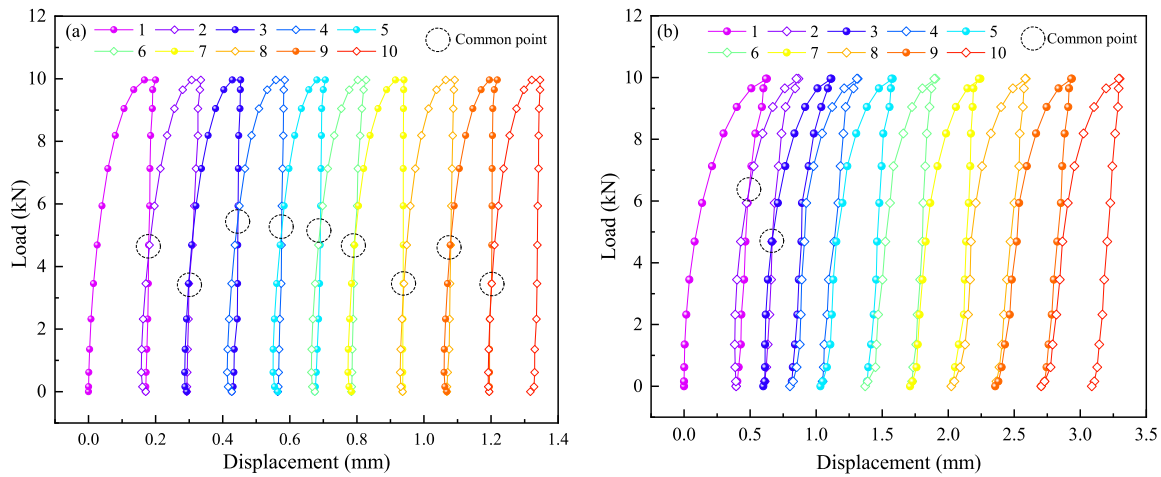
Fig. 19. Load-displacement curve with cyclic load amplitude of 10kN: (a) windblown sand ballast bed, (b) clean ballast bed.

become zero with the increasing load amplitudes. This shows that when the amplitude of lateral load exceeds 5kN, windblown sand ballast bed exhibits greater ability to resist lateral elastic deformation than the clean ballast bed.

The lateral stiffness of the ballast bed under varying loads is computed from Eq.16 to further analyze the influence of load amplitude on the lateral bearing capacity of the ballast bed.

$$k_i = \frac{F_c^i - F_c^0}{x_i - x_0} \tag{16}$$

In the equation, k_i is the lateral stiffness of the ballast bed under the load for the ith time; F_c^i and x_i are the peak load and sleeper lateral displacement value for the ith time respectively; F_c^0 and F_c^0 are the initial load and sleeper lateral displacement values respectively. The relationship among the plastic deformation accumulation, the lateral stiffness of the ballast bed and loading action times under varying load amplitudes is shown in Fig. 21.

It can be seen from Fig. 21(a) that with the increase in cyclic loading times and load amplitudes, the plastic deformation accumulation of the ballast beds in both types are gradually increasing but the plastic deformation accumulations and curve slope of the windblown sand ballast beds are comparatively lesser than those in the clean ballast beds. This indicates that the sand intrusion fills the voids between the ballasts, thus reducing the plastic deformation accumulation of the ballast beds. Fig. 21 (b) shows that the load times have little influence on the change of lateral stiffness of ballast beds in two types (except for the windblown

sand ballast bed at 5kN). As the load amplitude increases, the lateral stiffness of the two kinds of ballast beds decreases gradually. It is more evident in windblown sand ballast bed. In addition, from Fig. 21(b), it can be found that the lateral stiffness of the windblown sand ballast bed is greater than that of the clean ballast bed under varying load amplitudes, which indicates that the windblown sand ballast bed has strong load resistance. However, sand intrusion can increase the lateral stiffness of the ballast bed, enhance the lateral constraint of the sleeper, reduce the elasticity of the track structure, and affect the long-term service quality of the track structure.

Conclusions

The lateral resistance field tests of windblown sand railway are carried out and the 3-D discrete element model of sand ballast bed is established for analyzing the influence of sand intrusion on the evolution of the ballast bed lateral resistance. The conclusions are as follows as follows:

(1) Sand intrusion can increase the lateral resistance of the ballast bed. The mean lateral resistance of windblown sand ballast bed is 11.18 kN, which of clean ballast bed is 7.93 kN. By comparison, the lateral resistance of windblown sand ballast bed is approximately 40% higher than that of clean ballast bed. There are three stages in the lateral resistance evolution of clean ballast bed and windblown sand ballast bed, namely linear growth stage, nonlinear strengthening stage and yield stage.

(2) The work done by windblown sand ballast bed to overcome lateral resistance is mainly concentrated in nonlinear strengthening stage and yield stage, but relatively less in the linear growth stage. Compared with the clean ballast bed, the sandy ballast bed decreases the resistance work by 46% in the linear growth stage, but increases it by 83% and 37% respectively in the nonlinear strengthening stage and yield stage.

(3) With the increase in sleeper displacement, the contact force chain distribution of the windblown sand ballast bed is found to be more uniform except at the ballast shoulder part. The clean ballast bed is distributed primarily in the form of tree roots, among which the skeleton force chain function is more remarkable. Under same displacement levels, the resistance of ballast shoulder is greater than the resistance of sleeper bottom and crib ballast for the windblown sand ballast bed, while the sleeper bottom resistance is apparently higher than the ballast shoulder resistance and crib ballast resistance for the clean ballast bed. When the sleeper displacement is 2 mm, the resistance sharing
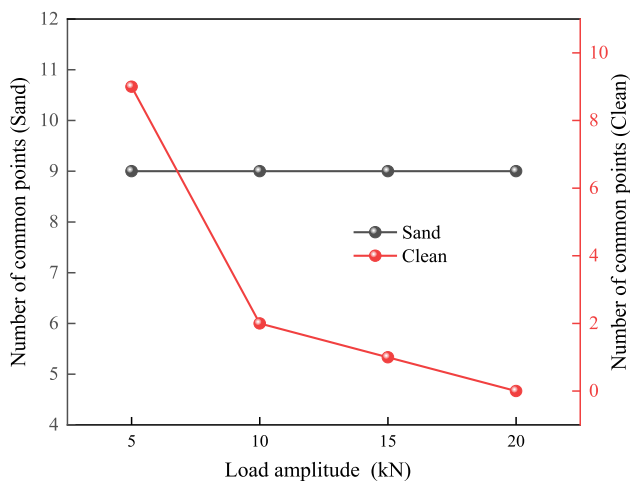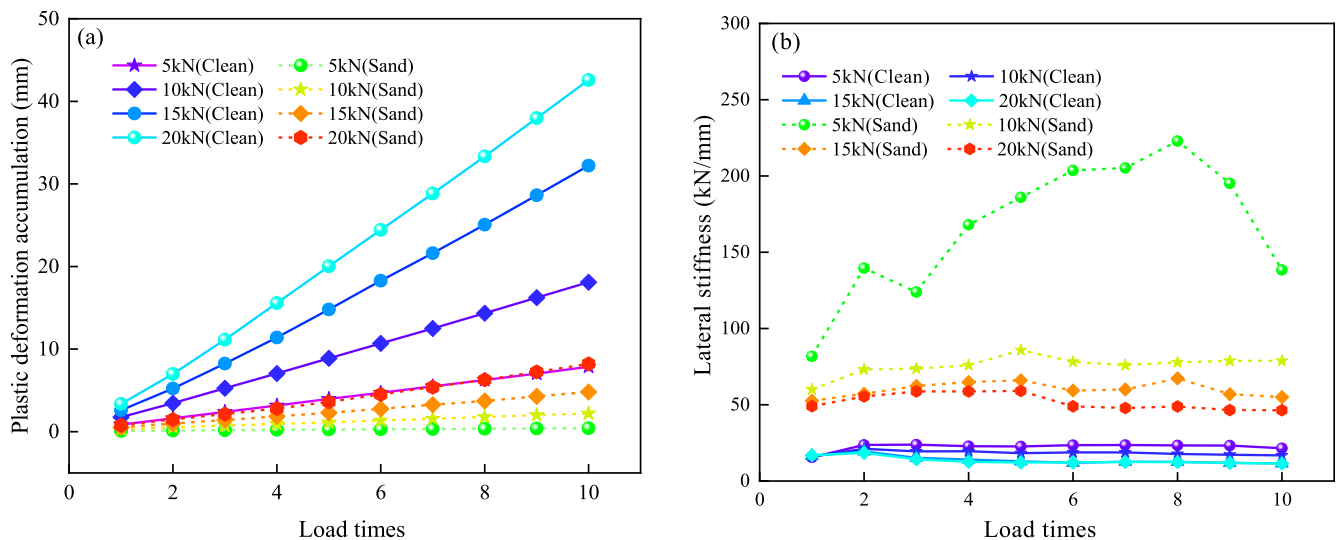

Fig. 20. Relationship curve between load amplitude and common points.

Fig. 21. Relationship curves between plastic deformation accumulation and lateral stiffness of the ballast bed with load times under different load amplitudes: (a) Plastic deformation accumulation, (b) Lateral stiffness of the ballast bed.

ratio of ballast shoulder, sleeper bottom and crib ballast are approximately 40%, 33% and 27% respectively.

(4) It is observed that greater the sand intrusion depth, higher is the resistance sharing ratio of ballast shoulder, the lateral resistance and resistance work. When the depth of sand intrusion is more than 0.35 m, increase in sand intrusion depth results in gradual increase of the ballast shoulder resistance and crib ballast, while the resistance of sleeper bottom is almost constant. When the sand intrusion depth is more than 0.44 m, the ballast shoulder resistance exceeds the sleeper bottom resistance and turns into the main component for the ballast bed lateral resistance.

(5) Increase in load amplitude leads to a reduction in the lateral stiffness of ballast beds in two types, in which windblown sand ballast bed decreases more. With the increase in cyclic load amplitude, the plastic deformation accumulation of windblown sand ballast bed is found to be smaller than that of clean ballast bed, and its slope of plastic deformation accumulation curve is also less. In addition, sand intrusion can increase the lateral stiffness of the ballast bed and reduce the elasticity of track structure.

CRediT authorship contribution statement

Zhihai Zhang: Project administration, Funding acquisition, Supervision, Methodology. **Hong Xiao:** Conceptualization, Formal analysis. **Yang Wang:** Software, Validation, Formal analysis. **Jia Fang:** Software, Data curation. **M.M. Nadakatti:** . **Haoyu Wang:** Data curation.

Declaration of Competing Interest

The authors declare that they have no known competing financial interests or personal relationships that could have appeared to influence the work reported in this paper.

References

[1] Zhang X, Zhao C, Zhai W. Importance of load frequency in applying cyclic loads to investigate ballast deformation under high-speed train loads [J]. Soil Dyn Earthquake Eng 2019;120(MAY):28–38.

[2] Esmaeili M, Shamohammadi A, Farsi S. Effect of deconstructed tire under sleeper pad on railway ballast degradation under cyclic loading [J]. Soil Dyn Earthquake Eng 2020;136:106265. https://doi.org/10.1016/j.soildyn.2020.106265.

[3] Bruno L, Horvat M, Raffaele L. Windblown sand along railway infrastructures: a review of challenges and mitigation measures. J. Wind Eng. Ind. Aerod. 2018;177: 340–65.

[4] Xiao H, Zhang Z, Cui X, Jin F. Experimental study and discrete element analysis of ballast bed with various sand content. J. Construction and Building Materials. 2021;271:121869. https://doi.org/10.1016/j.conbuildmat.2020.121869.

[5] Esveld C. Modern railway track. Zaltbommel: MRT; 2001.

[6] Liu J, Chen R, Liu Z, Liu G, Wang P, Wei X. Comparative analysis of resistance characteristics of composite sleeper and concrete sleeper in ballast bed.J. Constr Build Mater 2021;300:124017. https://doi.org/10.1016/j.conbuildmat.2021.124017.

[7] Liu J, Wang P, Liu G, Dai J, Xiao J, Liu H. Study of the characteristics of ballast bed resistance for different temperature and humidity conditions. J. Construction and Building Materials. 2021;266:121115. https://doi.org/10.1016/j.conbuildmat.2020.121115.

[8] Le Pen LM, Powrie W. Contribution of base, crib, and shoulder ballast to the lateral sliding resistance of railway track: a geotechnical perspective. J. Proc. Inst. Mech. Eng., Part F: J. Rail Rapid. Transit. 2011;225(2):113–28.

[9] Tutumluer E, Hai H, Hashash Y. Aggregate Shape Effects on Ballast Tamping and Railroad Track Lateral Stability. AREMA 2006 Annual Conference Louisville. 2006.

[10] Lu M, McDowell GR. The importance of modelling ballast particle shape in the discrete element method. J. Granular Matter. 2006;9(1-2):69–80.

[11] Jing G, Aela P, Fu H. The contribution of ballast layer components to the lateral resistance of ladder sleeper track. J Construction and Building Materials. 2019;202: 796–805.

[12] Jing G, Ji Y, Aela P. Experimental and numerical analysis of anchor-reinforced sleepers lateral resistance on ballasted track.J. Constr Build Mater 2020;264: 120197. https://doi.org/10.1016/j.conbuildmat.2020.120197.

[13] Jing G, Zhang Xu, Jia W. Lateral resistance of polyurethane-reinforced ballast with the application of new bonding schemes: Laboratory tests and discrete element simulations. J Construction and Building Materials 2019;221:627–36.

[14] Esmaeili M, Zakeri JA, Babaei M. Laboratory and field investigation of the effect of geogrid-reinforced ballast on railway track lateral resistance. J. Geotextiles & Geomembranes. 2017;45(2):23–33.

[15] Guo Y, Fu H, Qian Yu, Markine V, Jing G. Effect of sleeper bottom texture on lateral resistance with discrete element modelling. J. Construction and Building Materials. 2020;250:118770. https://doi.org/10.1016/j.conbuildmat.2020.118770.

[16] Kish A, Samavedam G. Dynamic buckling of continuous welded rail track: Theory, tests, and safety concepts. J. Transp. Res. Rec. 1991;1289:23–38.

[17] Kish A, Samavedam G. Improved destressing of continuous welded rail for better management of rail neutral temperature. J. Transp. Res. Rec. 2005;1916(1):56–65.

[18] Kabo E. A numerical study of the lateral ballast resistance in railway tracks. J. Proc. Inst. Mech. Eng., Part F: J. Rail Rapid. Transit. 2006;220(4):425–33.

[19] Zeng Z, Song S, Wang W, et al. Ballast bed resistance characteristics based on discrete-element modeling.J. Advances in Mechanical Engineering. 2018;10(6). 168781401878146.

[20] TolouKian AR, Sadeghi J, Zakeri J-A. Large-scale direct shear tests on sand-contaminated ballast. Proceedings of the Institution of Civil Engineers - Geotechnical Engineering 2018;171(5):451–61.

[21] Tolou Kian AR, Zakeri JA, Sadeghi J. Experimental investigation of effects of sand contamination on strain modulus of railway ballast. J. Geomechanics and Engineering. 2018;14(6):563–70.

[22] Tolou Kian AR, Sadeghi J, Zakeri J-A. Influences of railway ballast sand contamination on loading pattern of pre-stressed concrete sleeper. J. Construction and Building Materials. 2020;233:117324. https://doi.org/10.1016/j. conbuildmat.2019.117324.

[23] Zakeri JA, Esmaeili M, Fathali M. Evaluation of humped slab track performance in desert railways. Proceedings of the Institution of Mechanical Engineers, Part F: Journal of Rail and Rapid Transit 2011;225(6):566–73.

[24] Zakeri J-A, Esmaeili M, Mosayebi S, Abbasi A. Effects of vibration in desert area caused by moving trains. J. Journal of Modern Transportation. 2012;20(1):16–23.

[25] Zakeri JA, Abbasi R. Field investigation of variation of loading pattern of concrete sleeper due to ballast sandy contamination in sandy desert areas. J Journal of Mechanical Science and Technology. 2012;26(12):3885–92.

[26] Esmaeili M, Aela P, Hosseini A. Experimental assessment of cyclic behavior of sand-fouled ballast mixed with tire derived aggregates. J. Soil Dynamics & Earthquake Engineering. 2017;98:1–11.

[27] Esmaeili M, Ebrahimi H, Sameni MK. Experimental and numerical investigation of the dynamic behavior of ballasted track containing ballast mixed with TDA. Proceedings of the Institution of Mechanical Engineers, Part F: Journal of Rail and Rapid Transit 2018;232(1):297–314.

[28] Esmaeili M, Zakeri JA, Mosayebi SA. Effect of sand-fouled ballast on train-induced vibration. Int. J. Pavement Eng. 2014;15(7):635–44.

[29] Sadeghi J, Tolou Kian AR, Ghiasinejad H, Fallah Moqaddam M, Motevalli S. Effectiveness of geogrid reinforcement in improvement of mechanical behavior of sand-contaminated ballast.J. Geotext Geomembr 2020;48(6):768–79.

[30] Sadeghi J, Tolou Kian AR, Fallah M. Experimental Investigation of Mechanical Properties of Ballast Contaminated with Wet Sand Materials. J. International Journal of Geomechanics. 2021;21(1):04020241. https://doi.org/10.1061/(ASCE) GM.1943-5622.0001886.

[31] Koohmishi M, Palassi M. Effect of gradation of aggregate and size of fouling materials on hydraulic conductivity of sand-fouled railway ballast.J. Constr Build Mater 2018;167:514–23.

[32] Tennakoon N, Indraratna B, Rujikiatkamjorn C, et al. The role of ballast fouling characterris tics on the drainage capacity of rail substructure. Geotech. Test. J. 2012;35(4):629–40.

[33] Tyfour WR. Effect of moving sand as a ballast contaminant on rail corrugation: field experience.J. International. J Environ Eng 2014;6(1):15–28.

[34] Ionescu D, Fedele D, Trounce M, et al. Deformation and degradation characteristics of sand-contaminated railway ballast. development and maintenance. Stirlingshire: Civil-Comp Press; 2016.

[35] De Iorio A, Grasso M, Penta F, Pucillo GP, Rosiello V. Transverse strength of railway tracks: part 2. Test system for ballast resistance in line measurement.J. Frattura Ed Integrità Strutturale. 2014;8(30):578–92.

[36] Liu J, Wang P, Liu G, Xiao J, Liu H, Gao T. Influence of a tamping operation on the vibrational characteristics and resistance-evolution law of a ballast bed. J. Construction and Building Materials. 2020;239:117879. https://doi.org/ 10.1016/j.conbuildmat.2019.117879.

[37] Koc W, Wilk A, Chrostowski P, Grulkowski S. Tests on lateral resistance in railway tracks during the operation of a tamping machine. J. Proc. Inst. Mech. Eng., Part F: J. Rail Rapid. Transit. 2011;225(3):325–40.

[38] Jing GQ, Luo Q, Wang Z, et al. Micro-analysis lateral ballast resistance of seismic characteristics. J. Journal of Vibroengineering. 2014;16(1):533–44.

[39] Zakeri J-A, Mirfattahi B, Fakhari M. Lateral resistance of railway track with frictional sleepers. J Proceedings of the Institution of Civil Engineers. 2012;165(2): 151–5.

[40] Ling X, Xiao H, Liu G, Zhang M. Discrete element modeling of polyurethane-stabilized ballast under monotonic and cyclic triaxial loading. J. Construction and Building Materials. 2020;255:119370. https://doi.org/10.1016/j. conbuildmat.2020.119370.

[41] Xiao J, Liu G, Liu J, et al. Parameters of a discrete element ballasted bed model based on a response surface method. J. Journal of Zhejiang University - Science A: Applied Physics & Engineering. 2019;20(9):685–700.

[42] Guo Y, Markine V, Song J, Jing G. Ballast degradation: Effect of particle size and shape using Los Angeles Abrasion test and image analysis. J Construction & Building Materials. 2018;169:414–24.

[43] Xu Y, Gao L, Cai X, et al. Influences of ballast gradation on railway ballast bed dynamic characteristics based on laser scanning and discrete element method.J. Vib. Shock. 2017;36(5):127–33.

[44] Wang L, Wang X, Mohammad L, Abadie C. Unified method to quantify aggregate shape angularity and texture using Fourier analysis. J. Mater. Civ. Eng. 2005;17(5): 498–504.

[45] Zhou B, Wang J, Wang H. Three-dimensional sphericity, roundness and fractal dimension of sand particles. J. Géotechnique. 2018;68(1):18–30.

[46] Itasca Consulting Group, 2014. Inc., Particle Flow Code in 3 Dimensions, Minneapolis.

[47] Widulinski L, Kozicki R, Tejchman R. Numerical Simulations of Triaxial Test with Sand Using DEM. J. Archives of Hydroengineering & Environmental Mechanics. 2009;56(3–4):149–72.

[48] Cundall PA, Strack ODL. A discrete numerical model for granular assemblies.J. Géotechnique. 2008;30(3):331–6.

[49] Itasca Consulting Group Inc. PFC 5.0 documentation, User's Guide. Minneapolis. (2015).

[50] Ling X, Xiao H, Cui X. Analysis of mechanical properties of polyurethane-mixed ballast based on energy method.J. Constr Build Mater 2018;182(SEP.10):10–9.

[51] Gong J, Nie Z, Zhu Y, Liang Z, Wang X. Exploring the effects of particle shape and content of fines on the shear behavior of sand-fines mixtures via the DEM.J. Comput Geotech 2019;106:161–76.

[52] Geng J, Reydellet G, Clément E, Behringer RP. Green's Function Measurements of Force Transmission in 2D Granular Materials. J. Physica D: Nonlinear Phenomena. 2003;182(3-4):274–303.

[53] Howell WD. Stress distributions and fluctuations in static and quasi-static granular systems.J. Thesis Duke University. 1999;324.

[54] Liu H, Xiao J, Wang P, Liu G, Gao M, Li S. Experimental investigation of the characteristics of a granular ballast bed under cyclic longitudinal loading. J. Construction and Building Materials. 2018;163:214–24.

[55] Sinha BP, Gerstle KH, Tulin LG. Stress-Strain Relations for Concrete Under Cyclic Loading. J. Aci Structural Journal. 1964;62(2):195–210.

[56] Senetakis K, Payan M, Li H, Zamanian M. Nonlinear stiffness and damping characteristics of gravelly crushed rock: Developing generic curves and attempting multi-scale insights [J]. Transp Geotech 2021;31:100668. https://doi.org/ 10.1016/j.trgeo.2021.100668.

[57] Sandeep CS, Senetakis K. Micromechanical experiments using a new inter-granule loading apparatus on gravel to ballast-sized materials. J. Friction 2020;8(1):70–82.

[58] Reddy NSC, He H, Senetakis K. Huan He, Kostas Senetakis. DEM analysis of small and small-to-medium strain shear modulus of sands.J. Comput Geotech 2022;141: 104518. https://doi.org/10.1016/j.compgeo.2021.104518.

[59] Sandeep CS, Li S, Senetakis K. Scale and surface morphology effects on the micromechanical contact behavior of granular materials.J. Tribol Int 2021;159: 106929. https://doi.org/10.1016/j.triboint.2021.106929.

[60] Xiao H, Zhang Z, Chi Y, Wang M, Wang H. Experimental study and discrete element analysis on dynamic mechanical behaviour of railway ballast bed in windblown sand areas. Constr Build Mater 2021;304:124669. https://doi.org/10.1016/j. conbuildmat.2021.124669.